frontiers | Frontiers in Physics

TYPE Mini Review
PUBLISHED 05 November 2024
DOI 10.3389/fphy.2024.1488275

OPEN ACCESS

EDITED BY
Ralph Chamberlin,
Arizona State University, United States

REVIEWED BY
Aakansha,
Banasthali University, India

*CORRESPONDENCE
Raymond L. Orbach,
orbach@utexas.edu

RECEIVED 29 August 2024
ACCEPTED 07 October 2024
PUBLISHED 05 November 2024

CITATION
Zhai Q and Orbach RL (2024) Toward understanding the dimensional crossover of canonical spin-glass thin films.
Front. Phys. 12:1488275.
doi: 10.3389/fphy.2024.1488275

Toward understanding the dimensional crossover of canonical spin-glass thin films

Qiang Zhai[1] and Raymond L. Orbach[2]*

[1]MOE Key Laboratory for Nonequilibrium Synthesis and Modulation of Condensed Matter, School of Physics, Xi'an Jiaotong University, Xi'an, Shaanxi, China, [2]Texas Materials Institute, The University of Texas at Austin, Austin, TX, United States

Spin-glass thin films exhibit many features different from the bulk. The freezing temperatures of spin-glass films are suppressed for reduced thickness and follow the Kenning relation. The dynamics are altered near the vacuum interface. These phenomena are closely related to the lower critical dimension of spin glasses, the spin-glass correlation length, and the dimensional crossover from $d = 3$ to $d = 2$. In this article, we review the experimental facts and theoretical perspectives for spin-glass thin films. We focus on canonical spin-glass systems with the Ruderman–Kittel–Kasuya–Yosida (RKKY) interaction between magnetic impurities in a nonmagnetic host. Open questions to be addressed are emphasized.

KEYWORDS

spin glasses, dimensional crossover, freezing temperature, correlation length, interfacial effects

1 Introduction

Spin glasses [1] with random spin orientations yet strong correlations have motivated theoretical developments [2] to understand their emergent complexities and continue to spur new findings in complex systems [3]. After more than half a century of intensive efforts to uncover the physics of spin-glass dynamics, controversies remain. A consensus regarding the density of ground states and the stability of the spin-glass phase [4, 5] in an external field is still lacking.

Finite-size effects of spin glasses, first reported by the pioneering work of Kenning, Slaughter, and Cowen [6], offer a new route to uncover some of their mysteries. A surge of research interest in spin-glass thin films focuses on the dimensional crossover from $d = 3$ to $d = 2$ [7–14]. In this work, we review the experimental discoveries and theoretical developments for metallic canonical spin-glass thin films. The freezing temperature, T_f, one of the most studied quantities of thin films, is first introduced. The correlation length offers a unique lens through which to understand dimensional crossover. Simulations to extract the growth laws governing correlation lengths are introduced. We also examine the impact of the interface on the spin-freezing process. We conclude the paper with open questions and remarks.

2 The freezing temperature and dimensional crossover: experiments

The freezing temperature T_f [6, 7] of spin glasses is different from the critical temperature T_c. Approaching T_c from above in a bulk sample, a continuous symmetry

breaking in the phase space commences and signifies a phase transition. In thin film magnetometry measurements, T_f is defined as the temperature below which the zero-field-cooled (ZFC) magnetization, $M_{ZFC}(T,t)$, differs from the reference field-cooled magnetization $M_{FC}(T,t)$ (in some literature, T_f is defined as the peak of $M_{ZFC}(T,t)$; the difference between the two is small in a small enough magnetic field).

The time dependence of $M_{ZFC}(T,t)$ naturally leads to the time dependence of $T_f(t)$. When cooled from the paramagnetic phase to the working temperature T, $M_{ZFC}(T,t)$ exhibits a sudden jump after the field is switched on, and gradually increases toward $M_{FC}(T,t)$. $T_f(t)$ is, therefore, the highest temperature below which nonequilibrium dynamics set in for a fixed observation time t. In a domain growth model, the length scale sets the relaxation time. Consequently, the equality of relaxation time and observation time gives rise to the observed freezing temperature.

The technical difficulty of extracting T_f is the very weak magnetic signal of a thin film with dilute magnetic spins dispersed in a nonmagnetic host. To circumvent this issue, Kenning et al. [6] have used multilayers of CuMn thin films, separated by layers of either pure Cu or Si, to decouple the direct contact between the CuMn thin films. They found that T_f decreases monotonically as the CuMn film thickness is reduced. The data were originally fitted to the finite-size scaling form of Equation 1

$$T_c - T_f(L) \sim L^{-1/\nu_3}, \tag{1}$$

as proposed in the real-space droplet (domain) model, where L is the film thickness. The droplet model assumes the existence of two ground states of the spin-glass phase, related by time-reversal symmetry. The finite-temperature properties are governed by low-lying excitations of droplets of typical size ℓ. In response to Kenning's results, a new scaling ansatz for the free energy of the droplet in $d = 2$ was proposed, Equation 2,

$$F_\ell \sim \gamma \ell^{\theta_2}. \tag{2}$$

Because $\theta_2 < 0$, the spin-glass phase is unstable in $d = 2$, and long-range order is destroyed. Fisher and Huse [15] predicted that in the critical region,

$$\frac{T_c - T_f(L,t)}{T_c} \sim L^{-1/\nu_3}\left[\ln\left(t/L^{z_3}\right)\right]^{\left[\left(\psi_3+\nu_2\psi_2\theta_3\right)\nu_3\right]^{-1}}. \tag{3}$$

Equation 3 is difficult to test experimentally, as an accurate estimation of T_c is difficult. In addition, the error bars of the many exponents in Equation 3 contribute to the uncertainty of T_c.

An alternative interpretation of the freezing temperature was given in [12]:

$$\frac{T_f(L,t)}{T_g}\ln(t) \propto \ln(L/a_0), \tag{4}$$

where a_0 is the average spacing between the magnetic impurities, t is the experimental time scale, and T_g is the freezing temperature for the bulk sample. Equation 4 is referred to as the Kenning relation.

Figure 1 exhibits data for T_f/T_g plotted against film thickness from [12,16], and [17]. It is assumed that the equilibrium correlation length perpendicular to the film plane, $\xi_\perp$, has saturated at the film thickness L at the time t, indicative of a dimensional crossover.

Because the lower critical dimension d_l of spin glass is between 2 and 3 (exactly 2.5 for Edwards–Anderson spin glass [18]), the critical temperature is zero after a dimensional crossover from $d = 3$ to $d = 2$. The energy barrier height that governs the relaxation time was found to only depend on L in a temperature range of 1 K at $T \approx 0.9T_f$ up to film thickness of 20 nm [12]. Equation 4 indicates that T_f shifts to lower T with slower cooling rates, or longer t, which is qualitatively consistent with experimental observations (e.g., Figure 1).

Additional support for the dimensional crossover of spin-glass thin films was obtained through polarized neutron reflectometry (PNR) [19, 20]. An asymmetry parameter A, defined as

$$A = (R^+ - R^-)/(R^+ + R^-), \tag{5}$$

was measured for AuFe thin films, where R^+ and R^- are the reflectivities for the spin-up neutrons and spin-down neutrons, respectively. By fitting Equation 5 with a Parratt recursion formalism, the average magnetic moment for Fe atoms was obtained, as reproduced in Figure 2. In the high-temperature regime, $\overline{\mu_{Fe}}$ can be described by the Brillouin function, $B(J,x)$, where J is the angular momentum, and $x = \mu B/k_BT$ with μ being the magnetic moment of impurities.

Below 50 K, $\overline{\mu_{Fe}}$ deviates from $B(J,x)$, in a range of 0.5–1.3 μ_B for $L \geq 5$ nm. Exceptions are for $L = 2$ nm and $L = 1$ nm, which follow a paramagnetic line down to 2 K. In particular, for the 1 nm film, the measured magnetic moment 4.2 μ_B is very close to the value for non-interacting Fe atoms.

These measurements were performed in a very high magnetic field of 6 T. In large fields, the measured moment should correspond to a quasi-equilibrium spin-glass phase. Therefore, at large observation times and for ultra-thin film, Equation 4 implies a $T_f \approx 0$, consistent with the measurements. In addition, the freezing of the magnetic moment for the thicker films implies the existence of a spin-glass phase up to 6 T.

According to calculations based on an Ising model, an A-T line [21] exists for the $H - T$ phase diagram of spin glasses, while the droplet picture predicts that the spin-glass phase vanishes in a magnetic field. However, equilibrium states are difficult to access in laboratory experiments, leaving a lack of consensus on the nature of the spin-glass phase in the presence of a magnetic field [21, 22].

3 Correlation length growth and dimensional crossover: simulations

It has been shown through Monte Carlo (MC) simulations and finite-size scaling [23–27] that the correlation length ξ diverges at a finite temperature for a 3D-Ising Edwards–Anderson (EA) model with either Gaussian or bimodal interactions. Similar conclusions were reached for the 3D-Heisenberg spin glass [28, 29] with the aid of a much larger sample size. The 2D-Ising (Heisenberg) spin glass only exhibits a phase transition at $T = 0$, as shown by free energy calculations

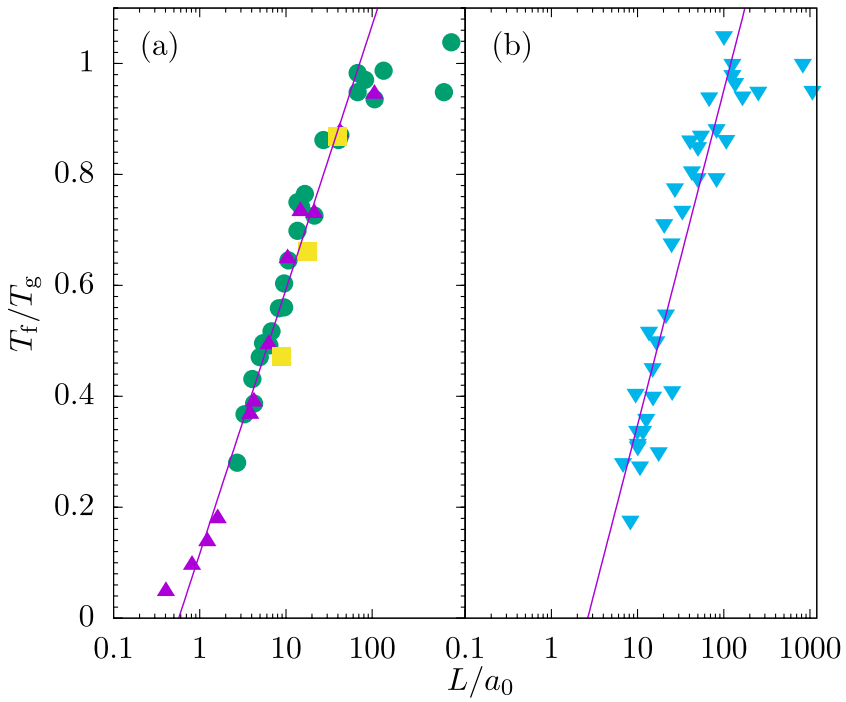

FIGURE 1
T_f collapses using Equation 4 for $L/a_0 \leq 100$. **(A)** Measurements of T_f for CuMn/Cu multilayer samples. The circle symbols represent data from [16], squares represent data taken from [12], and triangles indicate data taken from [17]. **(B)** T_f of CuMn multilayer films with a 7-nm Si interlayer.

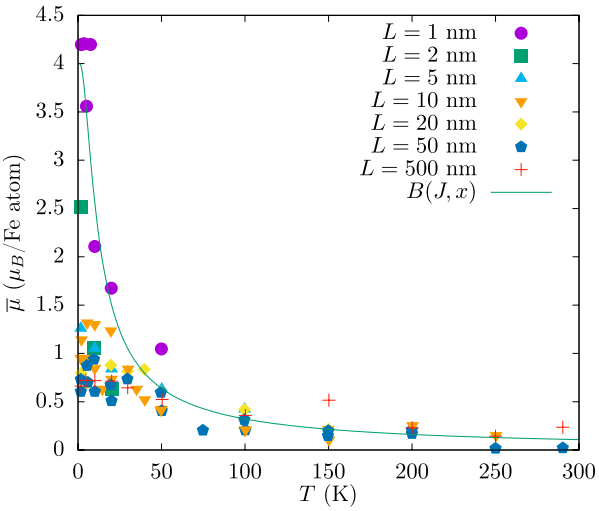

FIGURE 2
Averaged magnetic moment per Fe atom for AuFe films of different thickness L. A paramagnetic behavior is exhibited when L is reduced below 2 nm. Figure created based on the data of [19, 20].

[30] and MC simulations [31]. These findings imply that there must be a crossover of the spin-glass dynamics when the size of the system is reduced gradually by one dimension. Simulations are usually limited by sample size and time scales, but compared to experiments, they enjoy enhanced spatial resolutions and gain immediate access to spin configurations. They thus provide a unique route to understand dimensional crossover. In particular, they have been able to directly extract ξ.

Of particular interest is the aging dynamics of ξ when the spin-glass phase evolves from nonequilibrium towards equilibrium. In practice, simulations suddenly quench the sample from the paramagnetic state (infinite temperature) to a temperature comparable to experiments. Rieger et al. [32, 33] performed MC simulations on an Ising EA model with Gaussian interactions. In order to understand the aging phenomena observed in experiments, the autocorrelation function is introduced, defined by

$$C(t, t_w) = \frac{1}{N}\overline{\langle \sum_i S_i(t + t_w) S_i(t_w)\rangle}, \tag{6}$$

where t_w is the duration in which the sample remains at T after quench, and the averages are taken over thermal fluctuation and quenched disorder. For $t_w \gg \tau_{eq}$, $C(t, t_w)$ is stationary and only depends on t in Equation 6. For $t_w \ll \tau_{eq}$ and $t > t_w$, a power law of Equation 7 is found,

$$C(t, t_w) \propto t^{-\zeta(T)}. \tag{7}$$

$C(t, t_w)$ for different t_w obeys the simple scaling form,

$$\bar{c}\left(t/\tau(t_w)\right), \tag{8}$$

where $\tau(t_w) = t_w$ if $t_w \ll \tau_{eq}$. This is not consistent with activated dynamics,

$$\xi(t_w) \propto (\log t_w)^{1/\psi}, \tag{9}$$

which leads to a logarithmic scaling. The spatial correlation is calculated through Equation 10,

$$G(r,t_w)=\frac{1}{t_w}\sum_{t=t_w+1}^{2t_w}\overline{\langle S_0(t)S_r(t)\rangle^2}, \tag{10}$$

and the correlation length at t_w is given by Equation 11,

$$\xi(t_w)=2\int_0^\infty drG(r,t_w). \tag{11}$$

The growth of ξ can be fitted with the activated dynamics of Equation 9 or a power-law dynamics,

$$\xi(t_w)\propto t_w^{\alpha(T)}. \tag{12}$$

However, Equation 12 naturally leads to the scaling form of Equation 8 when assuming $C(t,t_w)\propto[\xi(t_w)/\xi(t)]^\lambda$, where $\lambda=\zeta(T)/\alpha(T)$. The power-law growth of ξ was later verified by Joh et al. [34].

A twelve-time-decade MC simulation of the Ising EA model was carried out by Fernandez et al. [13]. They clarified growth dynamics for ξ and reinforced the evidence for the scaling function of Equation 8. They found that, Equation 13,

$$\frac{\xi(t_w)}{\xi_{eq}}=\mathcal{G}\left(t_w/\tau(T)\right)+\mathcal{O}\left[(\xi(t_w))^{-\omega},\left(\xi_{eq}\right)^{-\omega}\right], \tag{13}$$

where ω is the corrections-to-scaling exponent, $\tau(T)\propto\exp(B/T^{1+\epsilon})$, and ϵ is a small number. This verified that the energy barrier height inferred from aging dynamics is physical [12].

The first MC simulation for dimensional crossover in a thin film geometry, comparable to experiments, was carried out by Victor Martin-Mayor and his coworkers [14]. The protocol used in this simulation closely resembled that of experiments: The sample was quenched to a working temperature, and the complete growth process (from nonequilibrium to equilibrium) of the correlation length was monitored. The correlation length is related to the autocorrelation function of Equation 14,

$$C_4(T,\boldsymbol{r},t)=\overline{\langle q^{(a,b)}(\boldsymbol{x},t)q^{(a,b)}(\boldsymbol{x}+\boldsymbol{r},t)\rangle}_T, \tag{14}$$

where $q^{(a,b)}(\boldsymbol{x},t)$ is the overlap between spin configuration $\sigma^{(a)}(\boldsymbol{x},t)$ and $\sigma^{(b)}(\boldsymbol{x},t)$ in replicas (a) and (b).

The estimator for the correlation length is given by Equation 15

$$\begin{aligned}\xi_\parallel(T,t)&=\int_0^\infty drr^2C_4(T,\boldsymbol{r},t)\Big/\int_0^\infty drrC_4(T,\boldsymbol{r},t),\\ \xi_\perp(T,t)&=\int_0^\infty drr^2C_4^\perp(T,\boldsymbol{r},t)\Big/\int_0^\infty drrC_4^\perp(T,\boldsymbol{r},t).\end{aligned} \tag{15}$$

Again, they found a power-law growth of the correlation length $\xi\propto t^{1/z}$.

Four time regimes were identified, with different z for $\xi_\parallel(T,t)$. In the first, $\xi_\parallel(T,t)$ grows with the aging rate $z_{d=3}$. Upon saturation of $\xi_\perp$ close to the film thickness h, the growth of $\xi_\parallel$ gradually speeds up in the second time regime. The aging rate of $\xi_\parallel$ in the third regime finally matches $z_{d=2}$, smaller than $z_{d=3}$ (faster dynamics). Finally, in the fourth regime, $\xi_\parallel$ reaches to its equilibrium value $\xi_\parallel^{eq}$.

Further analysis leads to a scaling function,

$$\frac{\xi_\parallel(t,T,L)}{\xi_{d=3}(t)}=\mathcal{F}\left[\xi_{d=3}(t,T)/L\right], \tag{16}$$

where $\xi_{d=3}(t)$ is the correlation length of a 3D sample. The invariance of Equation 16 allows a Kananoff–Wilson block spin transformation of the simulation results. These, in turn, lead to the mapping of the temperature of the film T to an effective temperature in $d=2$ (a true monolayer film),

$$\xi_\parallel^{eq}(T,L)=L\,\xi_{d=2}^{eq}\left(T_{d=2}^{eff}\right). \tag{17}$$

The mapping given by Equation 17 is remarkable in that an effective temperature can allow for treating the $3D$ spin-glass problem exactly in $2D$. For example, for $T\approx0.9T_c$, $T_{d=2}^{eff}\approx1.04T$. As the correction is negligible, the analyses of CuMn thin films in [12–14] are adequate.

4 Interfacial effects on spin freezing

Much of our understanding of dimensional crossover in thin films arises from multilayers of spin-glass films separated by non-magnetic metallic or insulating layers. It is natural to ask whether the interface between the spin-glass layers and the decoupling layers leads to artificial or unwanted effects. For example, as illustrated in Figure 1, the T_f of the same CuMn film decoupled by Si is lower than films decoupled by Cu [16]. The RKKY interaction, responsible for spin-glass behavior in metallic spin glasses, is mediated by the conduction electrons. This long-range interaction is sharply cut off at the CuMn/Si boundary but falls off slowly at the CuMn/Cu boundary [35], perhaps accounting for the difference. A quantitative analysis is lacking.

The first systematic study to address the effects of the decoupling layers was conducted by Granberg et al. [9]. They varied the thickness of Cu layers, L_i, to explore the freezing process of CuMn/Cu multilayers. We identify the T_f from Figure 1 of [9] in order to display the time dependence of T_f in Figure 3. The reduction of T_f follows a logarithmic time dependence given by Equation 4. The rates of reduction, $dT_f/d\log(t)$ for different L_i are displayed in Figure 4. The rate decreases with decreasing thickness of the decoupling layer until it reaches its $d=3$ value.

An explanation for the behaviors exhibited in Figures 3, 4 was given in [12]. For a given observation time, the inequality of Equation 18,

$$c_1a_0\left(\frac{t}{\tau_0}\right)^{c_2T/T_g}\le\xi_{eq}(T), \tag{18}$$

holds for $T\le T_f$ in $d=3$, where $\xi_{eq}(T)$ is the equilibrium correlation length obtained in the FC state. The growth of the correlation length for the ZFC protocol obeys the growth law on the left of Equation 18. For spin-glass films fully decoupled from one another, $\xi_\perp(t)$ is bounded by L regardless of T. $\xi_\parallel(t)$ grows faster than $\xi_\perp(t)$ [14]. Then, any films with $L\le\xi_{d=3}^{eq}(T)$ should be much more sensitive to the variation of the observation time scale. Between the $d=3$ and the fully decoupled layer limit, crosstalk occurs among the neighboring layers, leading to an intermediate sensitivity to the variation of observation time t.

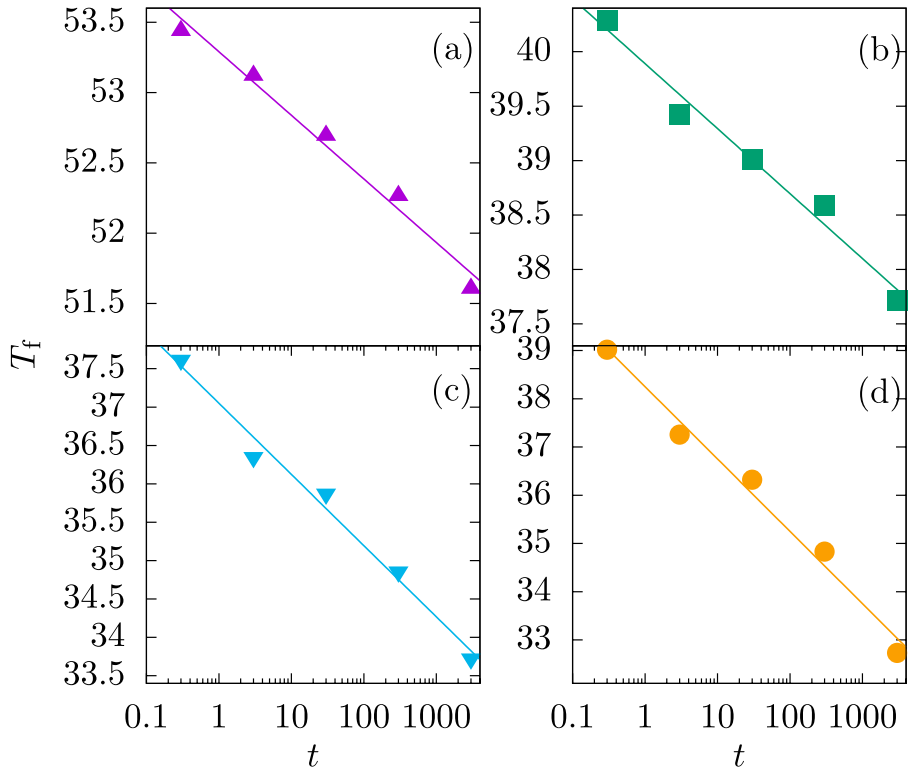

FIGURE 3
The freezing temperature decreases logarithmically with observation time t for CuMn/Cu multilayer thin films with interlayer thickness of **(A)** $L_i = 1$ nm, **(B)** $L_i = 7$ nm, **(C)** $L_i = 15$ nm, and **(D)** $L_i = 120$ nm.

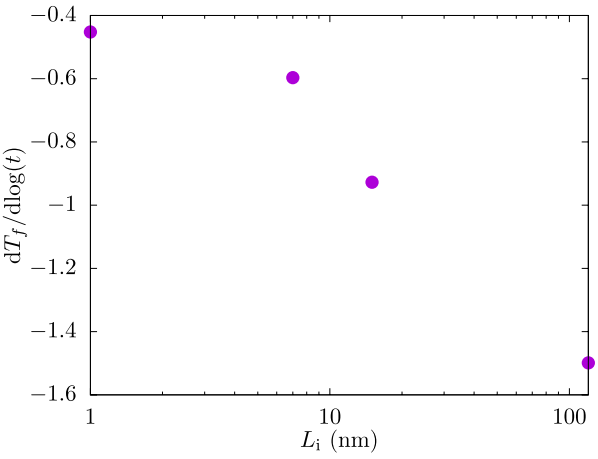

FIGURE 4
Changing rate of freezing temperature T_f versus the interlayer thickness L_i.

A direct probe of the surface dynamics has been carried out by depth-dependent muon-spin-relaxation (μSR) studies [36]. The μSR is a powerful technique to probe local spin orientations [37–39]. In the experimental setup, the polarized μ^+ beam is stopped by the sample, and the decay positron emitted from μ^+ is counted. The backward (EB) and forward (EF) counting rates are given by Equation 19,

$$N_{EF}(t) = N_F \exp(-t/\tau_u)[1 + G_z(t)],$$
$$N_{EB}(t) = N_F \exp(-t/\tau_u)[1 - G_z(t)], \quad (19)$$

where τ_μ is the lifetime of μ^+, and $G_z(t)$ is the muon-spin-relaxation function. $G_z(t) = 1$ for completely polarized spins, and $G_z(t) = 0$ for completely depolarized spins. The depolarization process can be inferred from the asymmetric time evolution of $N_{EF}(t)$ and $N_{EB}(t)$.

The muons are assumed to take random interstitial sites in the sample and do not diffuse in the lattice. For a CuMn (1 at%) sample, the atomic dipolar field (~100 G) from the Mn impurity dominates compared to the average RKKY field (~10 G) and the Cu nuclear dipolar field (~4 G). For an ordered translational invariant magnetic phase (e.g., a ferromagnet), the muon spin will precess with a single frequency in the local dipolar field. In the case of spin glasses, the randomness of the local dipolar field leads to a rapid depolarization of the polarized muons.

Taking into account the static random local fields and their fluctuation, a stochastic theory of muon-spin-relaxation for $G_z(t)$ was formulated by Uemura et al. [39]:

$$G_z(t) = \frac{1}{3}\exp\left[-\left(4a_d^2 t/\nu\right)^{1/2}\right] + \frac{2}{3}\left[1 - \frac{a_s^2 t^2}{\left(4a_d^2 t/\nu + a_s^2 t^2\right)^{1/2}}\right]\exp\left[-\left(4a_d^2 t/\nu + a_s^2 t^2\right)^{1/2}\right], \quad (20)$$

where $a_s = \sqrt{q_{EA}}a$ and $a_d = \sqrt{1 - q_{EA}}a$ with a are the average amplitude of random fields. It was assumed that, Equation 21,

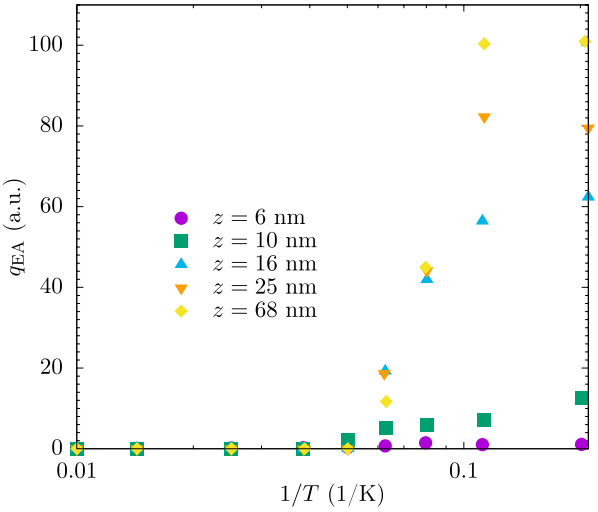

FIGURE 5
Self-overlap parameter, q_{EA}, plotted against $1/T$ at different depths of z from the vacuum interface for a 220-nm-thick AuFe film.

$$\overline{\langle S(t)S(0)\rangle} = (1 - q_{EA})\exp(-\nu t) + q_{EA}, \tag{21}$$

where the brackets represent thermal averages, and the bar indicates spatial averages. Each spin S has a preferred static component $\sqrt{q_{EA}}S$ below T_g, and a dynamic component $(1 - \sqrt{q_{EA}})S$ with a fluctuating rate ν.

Therefore, the order parameter q_{EA} [40] can be obtained by fitting Equation 20 to the experimental data. Figure 5 reproduced the extracted values of q_{EA} at different depth z of a 220-nm-thick AuFe film by [36]. At the low-temperature regime, q_{EA} attains a finite value, signifying the onset of spin freezing. The dynamical fluctuations of spins are significantly reduced with increasing distance from the surface. This suggests an inhomogeneous freezing gradient along the direction of the film thickness because of the vacuum interface. It is likely that the RKKY interaction between magnetic impurities is modified by the vacuum interface. However, again, a treatment to quantify this effect is lacking.

Recent $1/f$ noise measurements [41, 42], covering a much larger temperature window (inaccessible in magnetometry measurements) for a larger collection of film thicknesses, suggest that the maximum barrier height is temperature dependent for thicker films. Although this appears to conflict with the magnetometry measurements [12] at first glance, the $1/f$ noise is sensitive to the length scales associated with the electronic mean free path, which are much shorter than the range of the RKKY interaction. This may be the reason behind the discrepancy between the two experimental processes.

5 Conclusion

We have examined the evidence for dimensional crossover from $d = 3$ to $d = 2$ of spin-glass thin films. The results from the magnetometry and the PNR measurements are consistent with the Kenning relation, Equation 4. The correlation length serves as a caliber to quantify T_f. The $\log(t)$ dependence of T_f originates from the power-law growth of the correlation length, as detailed in large-scale simulations.

Although much has been understood concerning the dynamics of thin film spin-glasses, in our opinion, a few questions remain to be addressed:

(1) In the low-temperature regime of the spin-glass phase, the dynamics become too slow to be probed by magnetometry and simulations. The validity of the Kenning relation remains to be tested with novel experimental protocols or data analyses.
(2) Both the vacuum and Si interfaces alter the spin-freezing process. It remains unknown how the interface affects the spin correlations. A theoretical treatment of the interfacial effects would not only contribute to a deeper understanding of spin-glass physics but also would benefit devices utilizing junctions between spin-glasses and other magnetic ordering materials [43, 44].

Author contributions

QZ: writing–original draft and writing–review and editing. RO: writing–original draft and writing–review and editing.

Funding

The author(s) declare that financial support was received for the research, authorship, and/or publication of this article. QZ was supported by China Postdoc Fund Grant No. 2022M722548, Shaanxi NSF Grant No. 2023-JC-QN-0018, and Central University Basis Research Fund Grant No. xzy012023044. RO was supported by the U.S. Department of Energy, Office of Science, Basic Energy Sciences, Division of Materials Science and Engineering, under Award No. DE-SC0013599.

Conflict of interest

The authors declare that the research was conducted in the absence of any commercial or financial relationships that could be construed as a potential conflict of interest.

Publisher's note

References

1. Cannella V, Mydosh JA. Magnetic ordering in gold-iron alloys. *Phys Rev B* (1972) 6: 4220–37. doi:10.1103/PhysRevB.6.4220

2. Mézard M, Parisi G, Virasoro MA. *Spin glass theory and beyond: an introduction to the replica method and its applications*, 9. World Scientific Publishing Company (1987).

3. Charbonneau P, Marinari E, Parisi G, Ricci-tersenghi F, Sicuro G, Zamponi F, et al. Spin glass theory and far beyond: replica symmetry breaking after 40 years. *World Scientific* (2023). doi:10.1142/13341

4. Mézard M, Parisi G, Sourlas N, Toulouse G, Virasoro M. Nature of the spin-glass phase. *Phys Rev Lett* (1984) 52:1156–9. doi:10.1103/PhysRevLett.52.1156

5. Fisher DS, Huse DA. Ordered phase of short-range ising spin-glasses. *Phys Rev Lett* (1986) 56:1601–4. doi:10.1103/PhysRevLett.56.1601

6. Kenning GG, Slaughter JM, Cowen JA. Finite-size effects in a cumn spin-glass. *Phys Rev Lett* (1987) 59:2596–9. doi:10.1103/PhysRevLett.59.2596

7. Sandlund L, Granberg P, Lundgren L, Nordblad P, Svedlindh P, Cowen JA, et al. Dynamics of cu-mn spin-glass films. *Phys Rev B* (1989) 40:869–72. doi:10.1103/PhysRevB.40.869

8. Granberg P, Nordblad P, Svedlindh P, Lundgren L, Stubi R, Kenning G, et al. Dimensionality crossover in cumn spin-glass films. *J Appl Phys* (1990) 67:5252–4. doi:10.1063/1.344627

9. Granberg P, Mattsson J, Nordblad P, Lundgren L, Stubi R, Bass J, et al. Dynamics of coupled two-dimensional cu(mn) spin-glass films. *Phys Rev B* (1991) 44:4410–4. doi:10.1103/PhysRevB.44.4410

10. Wood G. The spin glass correlation length and the crossover from three to two dimensions. *J magnetism Magn Mater* (2010) 322:1775–8. doi:10.1016/j.jmmm.2009.12.028

11. Guchhait S, Orbach R. Direct dynamical evidence for the spin glass lower critical dimension $2 \leq dl \leq 3$. *Phys Rev Lett* (2014) 112:126401. doi:10.1103/PhysRevLett.112.126401

12. Zhai Q, Harrison DC, Tennant D, Dahlberg ED, Kenning GG, Orbach RL. Glassy dynamics in cumn thin-film multilayers. *Phys Rev B* (2017) 95:054304. doi:10.1103/PhysRevB.95.054304

13. Fernandez LA, Marinari E, Martin-Mayor V, Parisi G, Ruiz-Lorenzo JJ. An experiment-oriented analysis of 2d spin-glass dynamics: a twelve time-decades scaling study. *J Phys A: Math Theor* (2019) 52:224002. doi:10.1088/1751-8121/ab1364

14. Fernandez LA, Marinari E, Martin-Mayor V, Paga I, Ruiz-Lorenzo JJ. Dimensional crossover in the aging dynamics of spin glasses in a film geometry. *Phys Rev B* (2019) 100:184412. doi:10.1103/PhysRevB.100.184412

15. Fisher DS, Huse DA. Static and dynamic behavior of spin-glass films. *Phys Rev B* (1987) 36:8937–40. doi:10.1103/PhysRevB.36.8937

16. Kenning GG, Bass J, Pratt WP, Leslie-Pelecky D, Hoines L, Leach W, et al. Finite-size effects in cu-mn spin glasses. *Phys Rev B* (1990) 42:2393–415. doi:10.1103/PhysRevB.42.2393

17. Hoines L, Stubi R, Loloee R, Cowen JA, Bass J. How thin a spin glass is still a spin glass? *Phys Rev Lett* (1991) 66:1224–7. doi:10.1103/PhysRevLett.66.1224

18. Boettcher S. Stiffness of the edwards-anderson model in all dimensions. *Phys Rev Lett* (2005) 95:197205. doi:10.1103/PhysRevLett.95.197205

19. Saoudi M, Fritzsche H, Nieuwenhuys GJ, Hesselberth MBS. Size effect in the spin glass magnetization of thin aufe films as studied by polarized neutron reflectometry. *Phys Rev Lett* (2008) 100:057204. doi:10.1103/PhysRevLett.100.057204

20. Fritzsche H, van der Knaap JM, Hesselberth MBS, Nieuwenhuys GJ. Loss of spin glass behavior in ultrathin aufe films. *Phys Rev B* (2010) 81:132402. doi:10.1103/PhysRevB.81.132402

21. de Almeida J, Thouless D. Stability of the sherrington-kirkpatrick solution of a spin glass model. *J Phys A: Math Gen* (1978) 11:983–90. doi:10.1088/0305-4470/11/5/028

22. Young AP, Katzgraber HG. Absence of an almeida-thouless line in three-dimensional spin glasses. *Phys Rev Lett* (2004) 93:207203. doi:10.1103/PhysRevLett.93.207203

23. Palassini M, Caracciolo S. Universal finite-size scaling functions in the 3d ising spin glass. *Phys Rev Lett* (1999) 82:5128–31. doi:10.1103/PhysRevLett.82.5128

24. Ballesteros HG, Cruz A, Fernández LA, Martín-Mayor V, Pech J, Ruiz-Lorenzo JJ, et al. Critical behavior of the three-dimensional ising spin glass. *Phys Rev B* (2000) 62: 14237–45. doi:10.1103/PhysRevB.62.14237

25. Katzgraber HG, Körner M, Young AP. Universality in three-dimensional ising spin glasses: a Monte Carlo study. *Phys Rev B* (2006) 73:224432. doi:10.1103/PhysRevB.73.224432

26. Hasenbusch M, Pelissetto A, Vicari E. Critical behavior of three-dimensional ising spin glass models. *Phys Rev B* (2008) 78:214205. doi:10.1103/PhysRevB.78.214205

27. Baity-Jesi M, Baños RA, Cruz A, Fernandez LA, Gil-Narvion JM, Gordillo-Guerrero A, et al. Critical parameters of the three-dimensional ising spin glass. *Phys Rev B* (2013) 88:224416. doi:10.1103/PhysRevB.88.224416

28. Fernandez LA, Martin-Mayor V, Perez-Gaviro S, Tarancon A, Young AP. Phase transition in the three dimensional heisenberg spin glass: finite-size scaling analysis. *Phys Rev B* (2009) 80:024422. doi:10.1103/PhysRevB.80.024422

29. Baity-Jesi M, Fernández LA, Martín-Mayor V, Sanz JM. Phase transition in three-dimensional heisenberg spin glasses with strong random anisotropies through a multi-gpu parallelization. *Phys Rev B* (2014) 89:014202. doi:10.1103/PhysRevB.89.014202

30. Morgenstern I, Binder K. Magnetic correlations in two-dimensional spin-glasses. *Phys Rev B* (1980) 22:288–303. doi:10.1103/PhysRevB.22.288

31. Kawamura H, Yonehara H. Ordering of the heisenberg spin glass in two dimensions. *J Phys A: Math Gen* (2003) 36:10867–80. doi:10.1088/0305-4470/36/43/013

32. Rieger H, Steckemetz B, Schreckenberg M. Aging and domain growth in the two-dimensional ising spin glass model. *Europhysics Lett* (1994) 27:485–90. doi:10.1209/0295-5075/27/6/013

33. Rieger H, Schehr G, Paul R. Growing length scales during aging in 2d disordered systems. *Prog Theor Phys Suppl* (2005) 157:111–9. doi:10.1143/ptps.157.111

34. Joh Y, Orbach R, Wood G, Hammann J, Vincent E. Extraction of the spin glass correlation length. *Phys Rev Lett* (1999) 82:438–41. doi:10.1103/physrevlett.82.438

35. Kasuya T. s–d and s–f interaction and rare earth metals. Magnetism, 2. Academic Press New York (1966). 215–94.

36. Morenzoni E, Luetkens H, Prokscha T, Suter A, Vongtragool S, Galli F, et al. Depth-dependent spin dynamics of canonical spin-glass films: a low-energy muon-spin-rotation study. *Phys Rev Lett* (2008) 100:147205. doi:10.1103/PhysRevLett.100.147205

37. Uemura YJ, Yamazaki T, Hayano RS, Nakai R, Huang CY. Zero-field spin relaxation of μ^+ as a probe of the spin dynamics of AuFe and CuMn spin-glasses. *Phys Rev Lett* (1980) 45:583–7. doi:10.1103/PhysRevLett.45.583

38. Heffner R, Leon M, Schillaci M, MacLaughlin D, Dodds S. Muon spin relaxation studies of the spin glass agmn. *J Appl Phys* (1982) 53:2174–8. doi:10.1063/1.330771

39. Uemura YJ, Yamazaki T, Harshman DR, Senba M, Ansaldo EJ. Muon-spin relaxation in aufe and cumn spin glasses. *Phys Rev B* (1985) 31:546–63. doi:10.1103/PhysRevB.31.546

40. Edwards SF, Anderson PW. Theory of spin glasses. *J Phys F: Metal Phys* (1975) 5: 965–74. doi:10.1088/0305-4608/5/5/017

41. Harrison DC, Dahlberg ED, Orbach RL. Effect of anisotropy on 1/f noise measurements of cumn spin glasses. *Phys Rev B* (2019) 100:064411. doi:10.1103/PhysRevB.100.064411

42. Harrison DC, Dahlberg ED, Orbach RL. Extraction of the spin-glass free-energy landscape from 1/f noise measurements. *Phys Rev B* (2022) 105:014413. doi:10.1103/PhysRevB.105.014413

43. Ali M, Adie P, Marrows CH, Greig D, Hickey BJ, Stamps RL. Exchange bias using a spin glass. *Nat Mater* (2007) 6:70–5. doi:10.1038/nmat1809

44. Usadel KD, Nowak U. Exchange bias for a ferromagnetic film coupled to a spin glass. *Phys Rev B* (2009) 80:014418. doi:10.1103/PhysRevB.80.014418